Geochemistry of Major, Trace, and Rare Earth Elements in Biglar Permo-Triassic Bauxite Deposit, Northwest of Abgarm, Ghazvin Province, Iran

A.A. Calagari,[1,*] F. Kangarani,[1] and A. Abedini[2]

[1]*Geology Department, Faculty of Natural Sciences, Tabriz University, Tabriz, Islamic Republic of Iran*
[2]*Geology Department, Faculty of Sciences, Urmia University, Urmia, Islamic Republic of Iran*

Abstract

Biglar Permo-Triassic bauxite deposit is located in ~15 km northwest of Abgarm, southwest of Ghazvin province, west of central Iran. It consists of 8 stratiform and discontinuous bauxite lenses lying along the contact of Ruteh (Permian) and Elika (Triassic) carbonate formations. Petrographically, the bauxite ores exhibit collomorphic-fluidal, pseudo-breccia, pseudo-porphyritic, panidio-morphic-granular, nodular, and skeletal textures indicative of authigenic origin. Weathering of andesitic parent rocks led to the formation of Ferruginous laterite, bauxitic clay, and siliceous bauxite. Mass change calculations of elements indicate that Si, and Ba were depleted during bauxitization and Al, Ti, Zr, Nb, Hf, Ga, U, Th, V, and Cr were enriched. However, Fe, Y, Rb, Sr, Co, Ni, LREEs, and HREEs experienced leaching-fixation mechanism during the development of the residual system. Based upon obtained data, the available organic matters, pH variations in weathering solutions, adsorption process, functioning of carbonate bedrock as a geochemical barrier, existing in resistant minerals, and fixation in the neomorphic phases have been shown to play significant role in distribution of trace and rare earth elements. Further geochemical considerations indicate that minerals such as monazite, rhabdophane, belovite, churchite, and xenotime are the potential hosts for rare earth elements in Biglar bauxite deposit.

Keywords: Bauxite; Biglar; Ghazvin; Trace and rare earth elements; Neomorphic phases; Weathering

Introduction

Biglar area is located in ~15 km northwest of Abgarm, southwest of Ghazvin province in west of central Iran. Geographically, the area extends from 49°, 10' to 49°, 11' east longitude and from 35°, 50' to 35°, 51' north latitude (Fig. 1). The principal rock formations in the area, from oldest to youngest, include Lalun (sandstone), Mila (carbonate), Dorud (sandstone), Ruteh (carbonate), and Shemshak (shale and sandstone) (Fig. 1). Bauxite deposit at Biglar that is a part of bauxite province of central plateau of Iran was developed

* Corresponding author, Tel.: +98(411)3392699, Fax: +98(411)3356027, E-mail: calagari@tabrizu.ac.ir
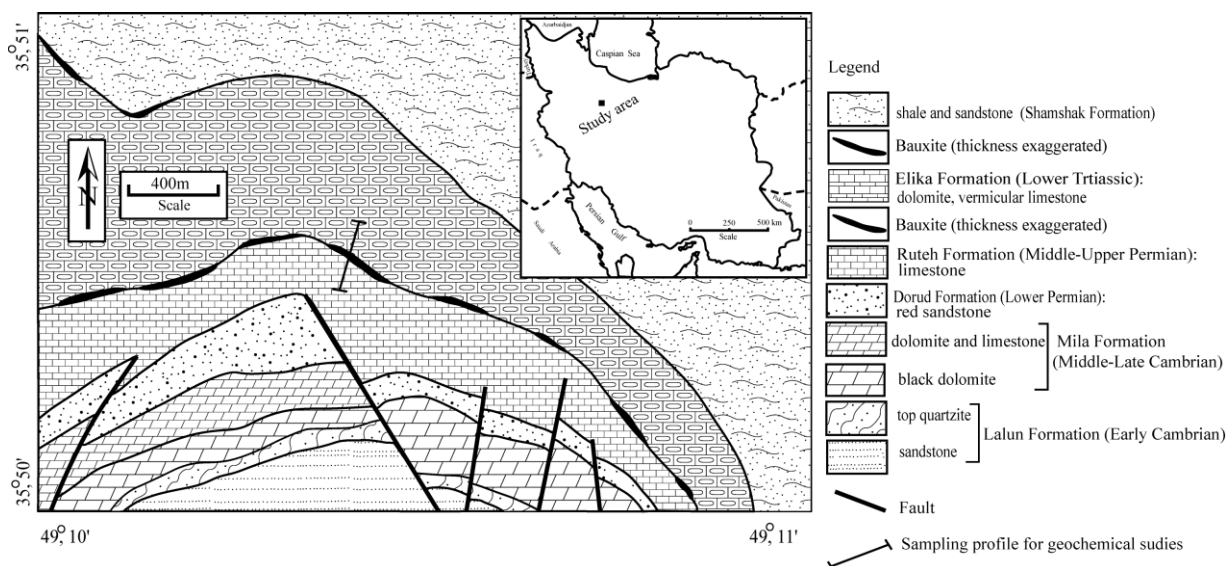
Figure 1. A geologic map illustrating the position of Biglar Permo-Triassic bauxite lenses.

temporally during two discrete periods, (1) Permo-Triassic and (2) upper Triassic.

Untill 2006, no genetic studies were done on Permo-Triassic bauxite horizon at Biglar. In early 2006, the present authors began to implement field and relatively comprehensive laboratory investigations on the subject. The preliminary results were presented in two separate national symposiums [10, 11]. However, this study focused chiefly on issues concerning origin, textural patterns, mineralogical and geochemical controls on distribution of major, trace and rare earth elements (REEs), and minerals hosting REEs.

Materials and Methods

Studies on Biglar Permo-Triassic bauxite deposit were carried out in two separate parts, (1) field and (2) laboratory. During field works, the attitude (dip and strike), thickness and relationships of bauxite lenses with the enclosing rocks in different parts of the area, and their genetic characteristics were considered. Because of lithological and physical variations, 60 samples from bauxite ores, footwall, hanging wall, and igneous rocks (present at the contact of ores with carbonate bedrock) were taken systematically across the strike of bauxite lenses.

Laboratory investigations were done after sample preparation. The mineralogy of ores was studied by petrographical examinations of 30 thin-polished sections, and also by applying X-ray Diffraction (XRD) method (9 samples) (see Table 1) carried out at

Geological Survey of Iran (GSI). Geochemical studies were implemented by bulk chemical analyses on 10 pulverized samples of various bauxite ores and the potential parent rock (see Table 2) by using ICP-MS method at Als-Chemex laboratories in Canada.

Discussion

Geology

Permo-Triassic bauxite horizon at Biglar consists of 8 discontinuous lenses with two overall trending, NW-SE and E-W (Fig. 1). The horizon lies along the contact of Ruteh and Elika carbonate formations and extends ~1.8 km with thicknesses ranging from 5 to 21 meters.

The significant geological aspects of the horizons are the presence of multi-color patterns on the surfaces of the ores (due to disharmonic dissolution of minerals) and remnants of igneous rocks existing along the contact of bauxite ores with carbonate bedrocks.

A profile across the strike of a selected bauxite lens was studied in detailed. Based upon physical characteristics, nine distinct bauxitic units were distinguished within this lens that are, from bottom to the top, (1) violet (VB), (2) red (RB), (3) orange red (ORB), (4) kaolinitic red (KRB), (5) multi-color (MCB), (6) Ferruginous gray (FGB), (7) yellow (YB), (8) gray (GB), and (9) white (WB) bauxites (Fig. 2). The followings are some outstanding geological features developed in Biglar bauxite ores:

1- The sharp contact existing between bauxite lenses

Table 1. The ICP-MS chemical analyses of bauxite (9) and andesite (1) samples from Biglar bauxite deposit

Sample No	A-1	Rs-1	Rs-2	Rs-3	Rs-4	Rs-5	Rs-6	Rs-7	Rs-8	Rs-9
Name of unit	Andesite	VB	RB	ORB	KRB	MCB	FGB	YB	GB	WB
SiO_2 (Wt%)	53.50	5.99	15.80	27.60	22.40	5.77	25.70	36.90	39.40	6.67
Al_2O_3	18.95	32.4	30.10	23.40	24.50	36.3	18.85	24.60	32.50	68.00
Fe_2O_3	6.63	45.3	34.50	32.00	34.10	36.5	32.80	16.10	1.58	0.83
CaO	6.16	0.15	0.28	0.26	0.32	0.26	0.15	2.11	0.29	0.22
Na_2O	5.58	0.10	0.20	0.10	0.30	0.2	0.30	0.70	0.10	0.30
MgO	2.66	0.05	0.20	0.14	0.22	0.1	0.31	0.95	0.16	0.18
K_2O	1.27	0.41	1.48	0.80	2.26	0.49	2.92	5.54	0.26	0.82
TiO_2	1.37	5.10	5.10	3.13	3.17	8.51	5.92	1.60	9.05	8.88
MnO	0.08	0.05	0.07	0.02	0.07	0.06	0.01	0.02	0.01	0.01
P_2O_5	0.38	0.12	0.34	0.24	0.56	0.14	0.13	0.03	0.11	0.16
L.O.I	1.47	9.76	9.66	10.40	9.96	9.66	11.55	10.40	14.45	11.95
Sum	98.20	99.50	98.0	98.30	98.40	98.2	98.80	99.30	98.00	98.30
U (ppm)	1.75	14.25	23.60	15.60	23.60	25.9	48.30	10.30	14.25	38.0
Th	3.02	7.64	11.25	7.74	10.20	9.80	14.15	21.80	9.75	16.55
Ba	503.00	62.10	166.00	86.70	268.00	123.50	229.0	398.0	62.10	47.60
Ga	19.70	57.80	50.90	29.80	35.70	32.10	33.30	45.20	57.80	92.40
Hf	4.60	15.40	10.50	8.10	10.00	12.90	12.60	7.60	15.40	19.10
Co	14.20	7.60	7.50	7.80	28.60	15.70	5.10	5.10	7.60	15.0
Cr	60.00	780.00	30.00	50.00	160.00	60.00	50.0	50.0	780.0	750.0
Nb	16.30	21.90	25.70	16.30	32.50	41.60	27.0	31.20	106.50	86.20
Rb	21.10	7.90	38.50	16.70	47.40	10.10	85.30	185.50	6.10	17.10
V	90.00	558.00	324.00	210.00	423.00	282.00	180.0	212.0	558.0	583.0
Y	27.20	17.10	41.00	43.10	52.00	22.70	40.80	40.0	17.10	31.50
Zr	184.00	622.00	431.00	315.00	355	485.00	522.0	295	622.0	707.0
Ni	21.00	5.00	8.00	57.00	168.00	5.00	5.00	162.0	201.0	34.0
Sr	457.00	361.00	2260	1345	4400	983	285.0	1025	135.50	953.0
La (ppm)	17.80	24.90	64.30	42.50	58.80	44.30	35.10	71.70	23.10	11.40
Ce	38.20	70.40	130.00	77.00	121.00	128.00	71.70	152.00	29.50	58.80
Pr	5.20	5.90	18.30	11.60	21.50	7.63	7.89	16.80	53.80	34.10
Nd	21.8	21.30	85.60	52.20	102.00	23.40	30.80	62.00	21.90	14.10
Sm	5.22	4.60	23.50	14.50	17.30	4.00	7.50	11.20	6.86	4.58
Eu	1.60	1.20	6.90	4.10	5.10	1.10	1.80	2.30	2.00	1.70
Gd	5.41	4.30	20.00	14.00	17.00	4.40	8.20	10.00	6.20	5.80
Tb	0.85	0.53	2.39	2.19	2.63	0.69	1.26	1.36	0.84	1.02
Dy	5.05	3.65	11.30	12.50	13.40	4.40	7.30	7.38	4.40	6.10
Ho	1.03	0.74	1.82	2.22	2.32	0.93	1.40	1.45	0.77	1.29
Er	2.96	2.05	5.12	6.05	5.80	2.62	4.00	4.66	1.99	3.54
Tm	0.47	0.34	0.66	0.88	0.85	0.39	0.56	0.65	0.29	0.54
Yb	2.95	1.63	4.52	5.53	4.82	2.32	3.57	4.22	1.84	3.29
Lu	0.46	0.25	0.62	0.77	0.68	0.35	0.52	0.62	0.26	0.49
LREE	95.23	132.00	346.00	216.00	342.00	212.00	162.00	325.00	94.60	99.40
HREE	13.77	9.19	26.40	30.00	30.50	11.70	18.70	20.30	10.30	16.30
REE	109.00	141.19	372.40	246.00	372.50	223.70	180.70	345.30	104.90	115.70

Table 2. Constituent minerals identified by XRD method in various bauxitic units in Biglar bauxite deposit

Sample No	Bauxitic units	Mineral identified	
		Major	*Minor*
Rs-1	White bauxite (WB)	Diaspore, Anatase, Feldspar	Kaolinite, Muscovite
Rs-2	Gray bauxite (GB)	Kaolinite, Anatase	Feldspar, Quartz
Rs-3	Yellow bauxite (YB)	Muscovite, Goethite, Calcite	Diaspore, Feldspar, Kaolinite
Rs-4	Ferruginous gray bauxite (FGB)	Kaolinite, Hematite	Muscovite, Kaolinite
Rs-5	Multicolor bauxite (MB)	Hematite, Diaspore	Kaolinite
Rs-6	Kaoliniic red bauxite (KRB)	Hematite, Muscovite, Pyroxene	Kaolinite, Zeolite
Rs-7	Orange red bauxite (ORB)	Hamatite, Kaolinite	Goethite, anatase
Rs-8	Red bauxite (RB)	Diaspore, Hamatite, Anatase	Kaolinite
Rs-9	Violet bauxite (VB)	Diaspore, Hematite, Anatase	Kaolinite

and the enclosing rocks.

2- The presence of liesegang texture in multi-color bauxite unit.

3- Folding in some units (e.g., GB, YB, WB).

4- The presence of ample amounts of organic matters in YB.

5- The presence of fault mirrors on the surface of outcrops in some units (e.g., RB, ORB, KRB).

6- Growth of botryoidal goethite aggregates along with calcite and limonite on the surface of ores in ORB unit.

7- Gradual increase in density and hardness of bauxite units downwardly toward the footwall.

Petrography and Mineralogy of Bauxite Profile

The results of XRD analyses revealed that minerals such as diaspore, hematite and kaolinite constitute substantial portion of the rock volume. However, lesser amounts of goethite, muscovite, feldspar, anatase, pyroxene, lepidochrosite, calcite, zeolite, and quartz are also present (Table 2). According to microscopic examinations, the mineral aggregates in bauxite lenses show collomorphic-fluidal (Fig. 3a), pseudo-breccia, pseudo-porphyritic, panidiomorphic-granular, nodular, and skeletal (Fig. 3b) textures suggestive of an authigenic deposition [3]. The presence of stretched and flattened nodules is indicative of strong effect of epigenetic processes. Ooidic and pisoidic textures are not pronounced while hematitic nodules particularly in lower parts of the bauxite lenses were well-developed. The development of this type of textural pattern may be due to the continuous variation of underground water table and formation of ores in a relatively stagnant aqueous environment [28]. Abundant joints and fractures, being common features of epigenetic

processes in most bauxite deposits, are also present and spatially and temporally are divided into two groups. Those of the first group are restricted only within texture-forming units (e.g., pisoids) and are not extended into the surrounding matrix. They have radial patterns (particularly in pisoids) and are thought to have been developed as the result of primary compaction of bauxite-forming gels [4]. Joints of the second group, however, are spread in the matrix and could have two origins, (1) tectonic and (2) desiccation of the primary bauxite-forming gels.

Bauxite Lithology

Based upon the trivariate plot of $(Al_2O_3+TiO_2)$-Fe_2O_3-SiO_2 [1], the geochemical data at Biglar shows that the bauxite ores range in composition from ferruginous laterite (mainly in lower and middle units e.g., KRB, RB, VB) through bauxitic clay (mainly in upper and middle units e.g., GB, YB, FGB, ORB) to siliceous bauxite (exclusively in WB) (Fig. 4).

Parent Rocks and Their Mineralogy

The igneous rocks present at the lower contact of bauxite lenses with carbonate bedrocks have andesitic composition. Petrographically, they show porphyritic (Fig. 5), poikilitic and fluidal textures and contain phenocrysts of plagioclase, pyroxene, and opaque minerals. Plagioclase (65-70%) is mainly andesine, and partially altered to sericite, chlorite, and epidote. Pyroxene (15-20%) is uralitized to amphibole. Opaques (~10%) are chiefly pyrite and ilmenite. These rocks are considered to have proper composition and be competent as potential precursor for Biglar bauxite deposit. In this study, distribution values of trace
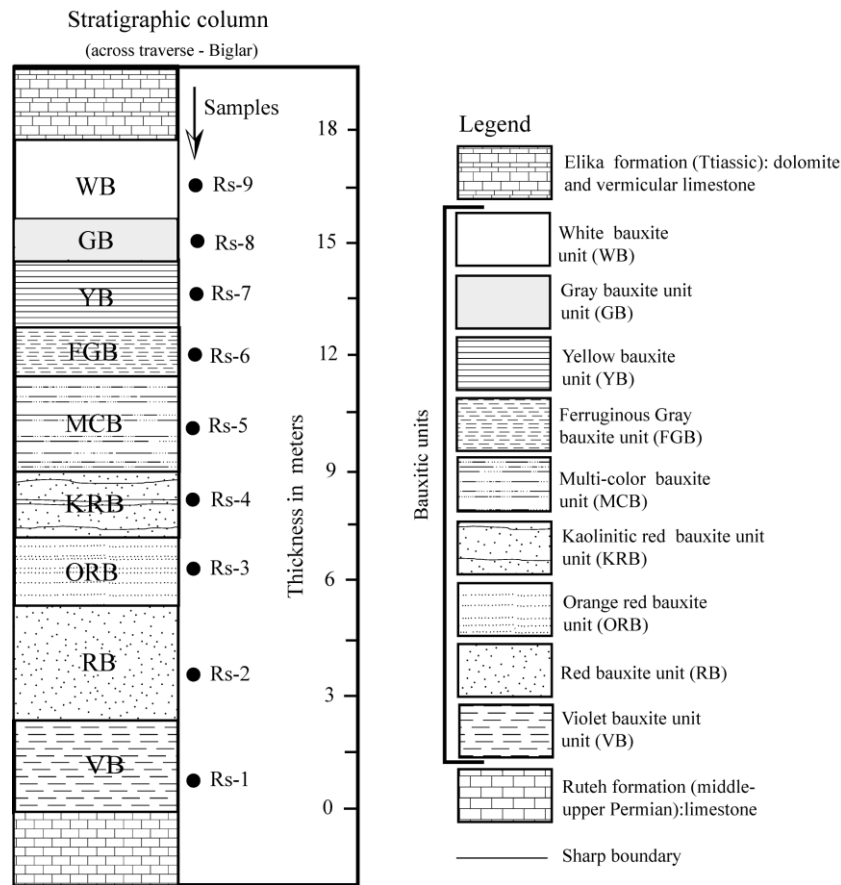
Figure 2. Stratigraphic column along a selective profile across Permo-Triassic bauxite lense at Biglar (for position see Fig. 1) with indication of analysed samples.
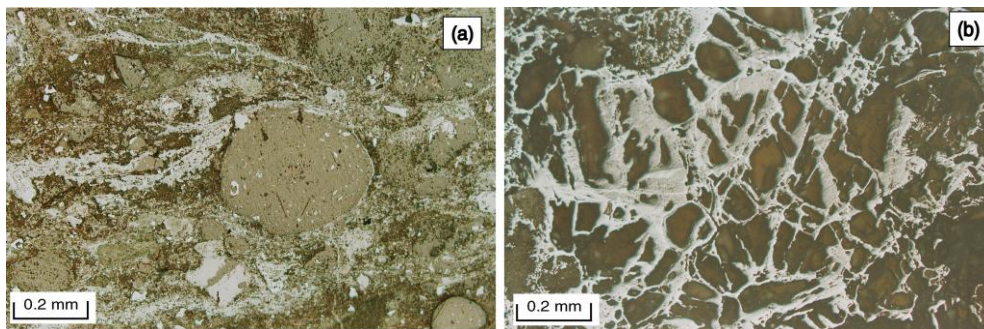

Figure 3. Photomicrographs of bauxitic samples: (a) collomorphic-fluidal texture; (b) skeletal texture.

elements were employed for consideration of the likely relationship between these rocks and the bauxite horizon. According to the trivariate plot of Ga-Cr-Zr [20], the parent rock should have a composition close to the intermediate igneous rock (Fig. 6a). The ratios of Zr/Ti and Nb/Y of parent rocks commonly remain constant during bauxitization [17, 9]. By virtue of this premise, the Biglar data on (Nb/Y)−(Zr/TiO$_2$) plot [31] indicate that the parent rocks might have compositions ranging from andesite to basaltic-andesite (Fig. 6b).
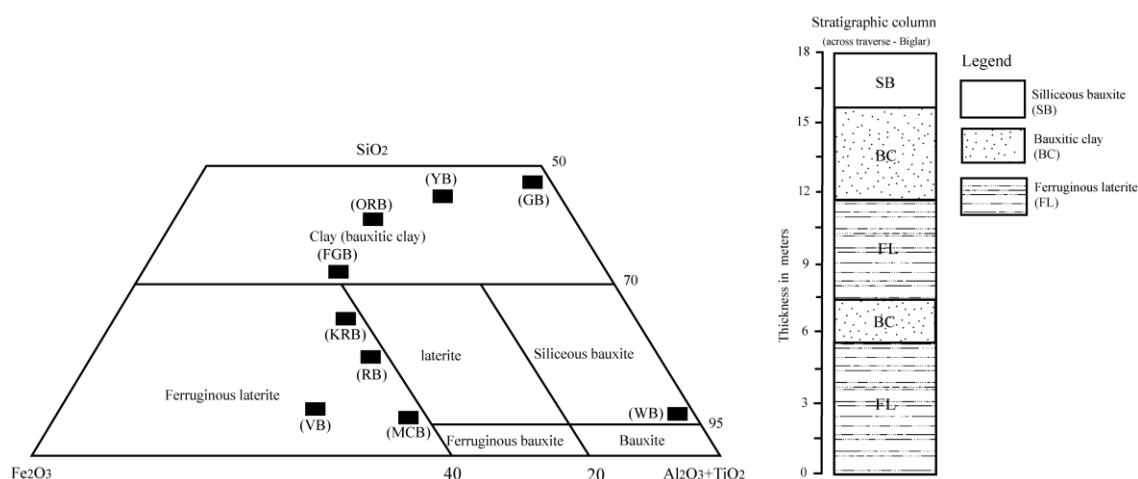
229

Figure 4. Ternary plot for the system of SiO_2, Fe_2O_3, and $(Al_2O_3+TiO_2)$ [1] showing the position of Biglar data points.

Mobility and Redistribution of Elements during Bauxitization

By pointing to an authigenic origin and andesitic parent rocks for this deposit, the geochemical processes involved during bauxitization can be envisaged by studies on mass changes of elements. Commonly elements such as Nb, Ti, Zr, Al, Th, and Hf are considered to be immobile under weathering conditions. They may be used as monitor immobile elements [29, 30]. However, the recent studies have proven that these elements can undergo mobilization to some extent under certain conditions during weathering [5, 18]. For this reason, none of these elements was used for mass change calculations in this study. Therefore, mobility and redistribution of elements were considered by applying the following equation proposed by Malpas et al. [18]:

$$\%change = 100\times [Element_{bauxite}/Element_{andesite}]-1]$$

The mass changes of elements calculated in this way (Table 3), were interpreted in five separate groups of elements (Figs. 7−11).

Major Elements (Al, Si, Fe, Ti)

The evolution of the bauxite profile was favored by overall mass increase in Al and Ti (Fig. 7a, b) and a decrease in Si (Fig. 7c). Fe was leached from the upper parts of the profile and shows enrichment in the lower parts (Fig. 7d). According to the mineralogy of andesitic precursor, Al was derived principally from the weathering of feldspars. The enrichment of Ti in the profile is due likely to the coupled break down of the original Ti-bearing minerals (e.g., pyroxene and ilmenite) and formation of new Ti mineral phases (e.g., rutile, anatase) during weathering. Fe seems to be derived from pyrite oxidation and weathering of pyroxene and ilmenite. Mass decrease of Si took place by the removal of silicic acid (formed during kaolinization or sericitization of feldspars and breakdown of kaolinite) from the residual system [12]. Formation of iron-organic complexes may be figured out by the presence of organic matters particularly in the upper parts of the profile. Transportation of these complexes by downward percolation of acid weathering solutions was the main cause for Fe removal from the upper parts of the profile. Creation of local reduced conditions by decaying organic matters was another important parameter which might have brought about depletion of Fe in the upper parts of the profile [19].
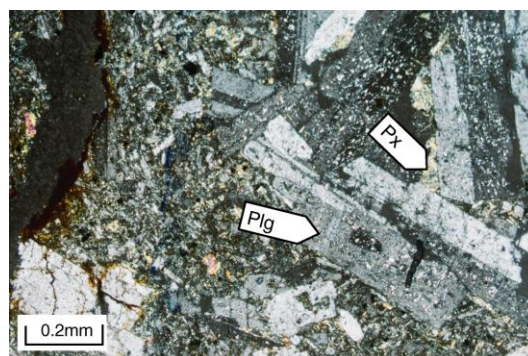

Figure 5. A photomicrograph of andesite with characteristic porphyritc texture. Plg = plagioclase and Px = Pyroxene.
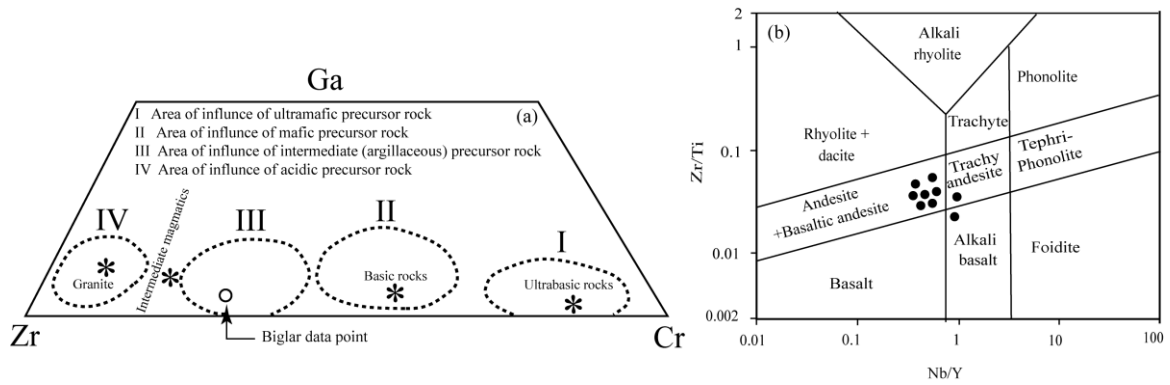
Figure 6. (a) A ternary plot for the concentration of Ga, Zr, and Cr [20], showing Biglar data point. (b) A bivariate plot of (Zr/Ti)-(Nb/Y) [31], depicting the Biglar data points.

Table 3. Mass changes of elements in different units of Biglar bauxite deposit

Sample No	Rs-1	Rs-2	Rs-3	Rs-4	Rs-5	Rs-6	Rs-7	Rs-8	Rs-9
Name of unit	VB	RB	ORB	KRB	MCB	FGB	YB	GB	WB
SiO_2	-88.80	-70.47	-48.41	-58.13	-89.21	-51.96	-31.03	-26.36	-87.53
Al_2O_3	70.98	58.84	23.48	29.29	91.56	-0.53	29.82	71.50	258.84
Fe_2O_3	583.26	420.36	382.65	414.33	450.53	394.72	142.84	-76.17	-87.48
TiO_2	272.26	272.26	128.47	131.39	521.17	332.12	16.79	560.58	548.18
U	714.29	1248.57	791.43	1248.57	1380.00	2660.00	488.57	714.29	2071.43
Th	152.98	272.52	156.29	237.75	224.50	368.54	621.85	222.85	448.01
Ba	-87.65	-67.00	-82.76	-46.72	-75.45	-54.47	-20.87	-87.65	-90.54
Ga	193.40	158.38	51.27	81.22	62.94	69.04	129.44	193.40	369.04
Hf	234.78	128.26	76.09	117.39	180.43	173.91	65.22	234.78	315.22
Co	-46.48	-47.18	-45.07	101.41	10.56	-64.08	-64.08	-46.48	5.63
Cr	1200.00	-50.00	-16.67	166.67	0.00	-16.67	-16.67	1200.00	1150.00
Nb	34.36	57.67	0.00	99.39	155.21	65.64	91.41	553.37	428.83
Rb	-62.56	82.46	-20.85	124.64	-52.13	304.27	779.15	-71.09	-18.96
V	520.00	260.00	133.33	370.00	213.33	100.00	135.56	520.00	547.78
Y	-37.13	50.74	58.46	91.18	-16.54	50.00	47.06	-37.13	15.81
Zr	238.04	134.24	71.20	92.93	163.59	183.70	60.33	238.04	284.24
Ni	-76.19	-61.90	171.43	700.00	-76.19	-76.19	671.43	857.14	61.90
Sr	-21.01	394.53	194.31	862.80	115.10	-37.64	124.29	-70.35	108.53
LREE	38.61	263.33	126.82	259.13	122.62	70.11	241.28	-0.66	4.38
HREE	-33.26	91.72	117.86	121.50	-15.03	35.80	47.42	-25.20	18.37

The mode of Fe distribution indicates that downward percolation of acid weathering solutions toward carbonate bedrocks caused coupled pH increase and Fe precipitation (as oxides and hydroxides) in lower units of the profile. Rising of underground water table could also play an important role in these processes.

High Field Strength Elements (Zr, Nb, Hf, Y, Ga)

Evolution of the bauxite profile was favored by mass increase of elements such as Zr, Nb, Hf, and Ga (Fig. 8a, b, c, d). Y experienced the leaching-fixation mechanism (Fig. 8e). The relative similarities among mass change patterns of Zr, Nb, Hf (Fig. 8a,b,c) and Ti
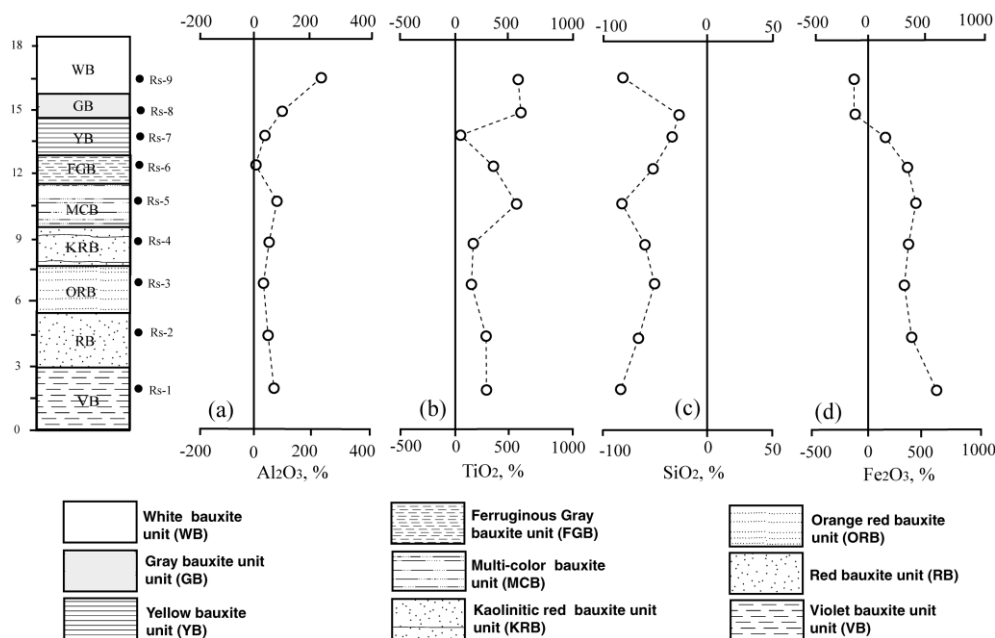
Figure 7. Mass change patterns for (a) Al$_2$O$_3$, (b) TiO$_2$, (c) SiO$_2$, and (d) Fe$_2$O$_3$ arcoss the studied profile at Biglar.
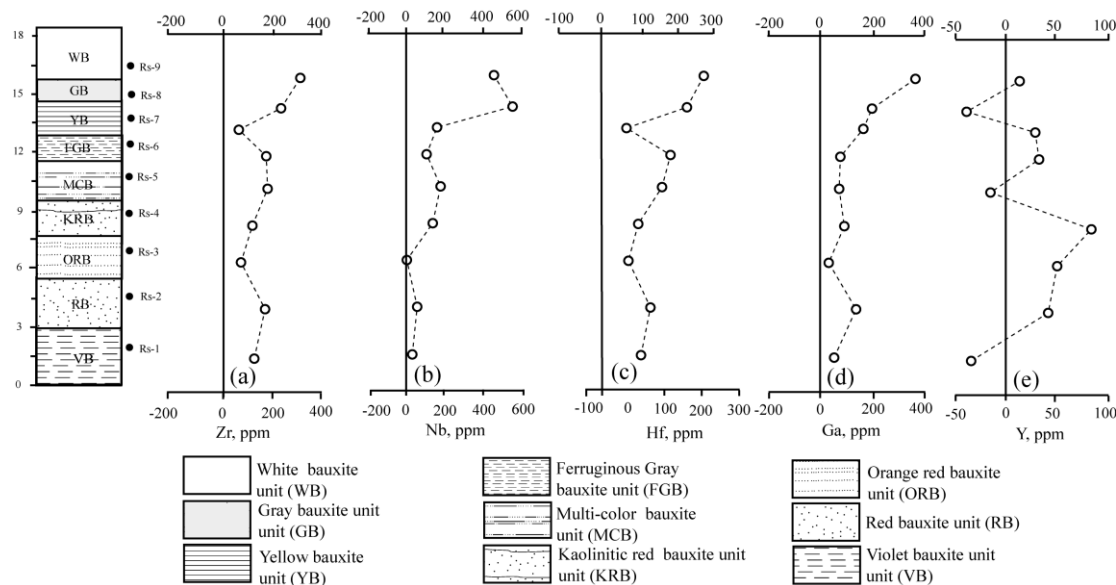

Figure 8. Mass change patterns for (a) Zr, (b) Nb, (c) Hf, (d) Ga, and (e) Y arcoss the studied profile at Biglar.

(Fig. 7b) indicates that the distribution of these elements was controlled by zircon and anatase [15]. The high correlation between P$_2$O$_5$ and Y (R= 0.88) shows that xenotime and churchite were likely the main fixation agent for Y. The relatively good correlation between Ga and Al (R= 0.66) may testify to the presence of Ga in the crystal lattice of diaspore.

Large ion Lithophile Elements (Rb, Ba, Sr, U, Th)

Rb and Sr exhibit fluctuating and irregular mass changes (Fig. 9a, b), whereas U and Th show overall enrichment (Fig. 9c, d). Ba suffered conspicuous depletion (Fig. 9e). The mass decrease of Rb, Sr, and Ba can be due to the alteration of feldspars in the parent rocks and their leaching by the weathering solutions.
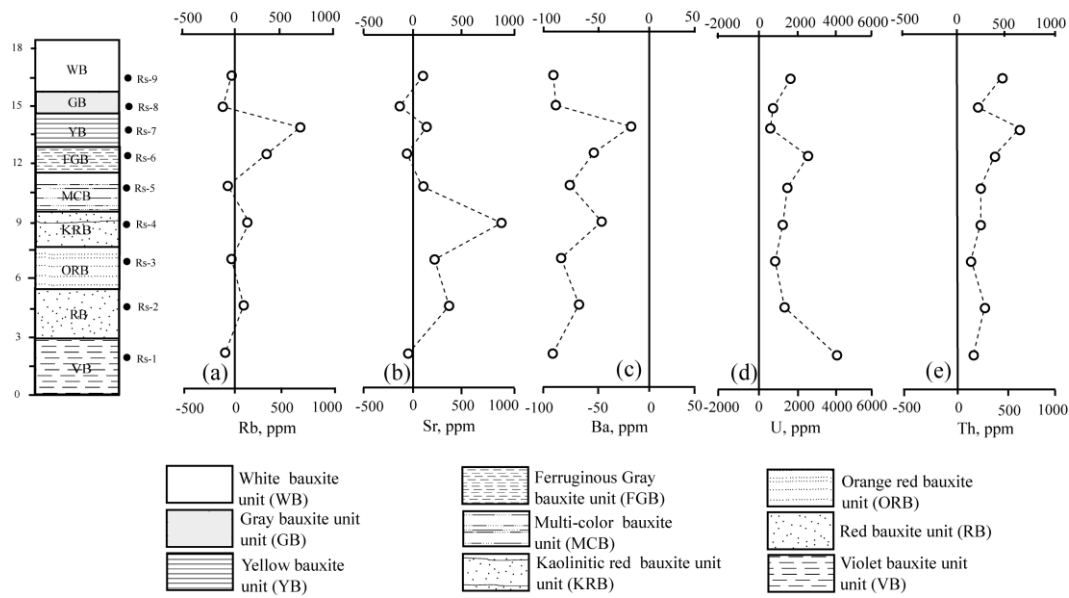
Figure 9. Mass change patterns for (a) Rb, (b) Sr, (c) Ba, (d) U, and (e) Th arcoss the studied profile at Biglar.
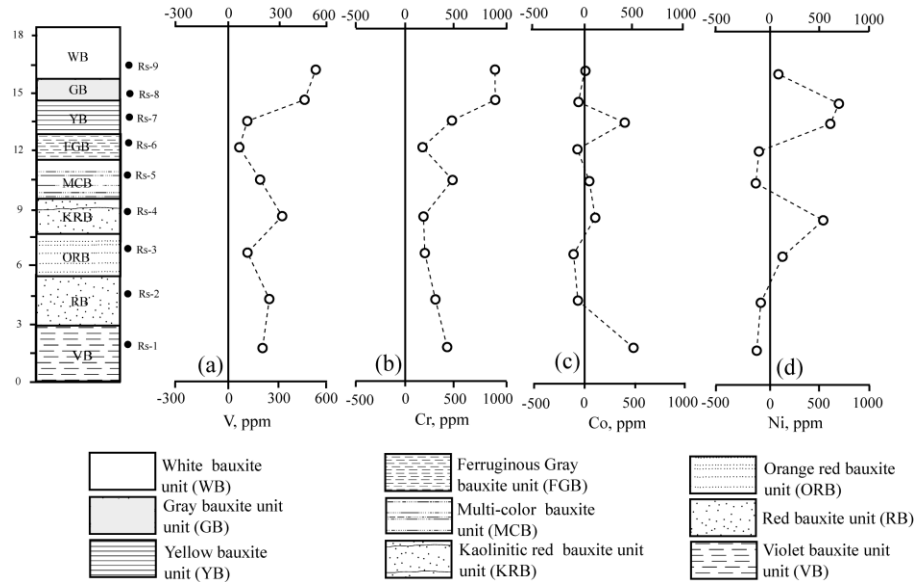

Figure 10. Mass change patterns for (a) V, (b) Cr, (c) Co, and (d) Ni arcoss the studied profile at Biglar.

Enrichment of Rb and Sr in some units within the profile may be owing to their adsorption by kaolinite [22]. Sr features conspicuously high positive correlation with P_2O_5 (R=0.95) and Ce (R= 0.71). This may be because of the fixation of Sr in some phosphate minerals (e.g., belovite, $[(Sr,Ce,Na,Ca)_5(PO_4)_3(OH)]$) [8]. The relatively good correlation between U and Fe (R= 0.65) may attest to the important roles of iron oxides and hydroxides (as controlling agents) in distribution of U within the weathered system [19, 16]. The pattern of mass increase of Th (Fig. 9d) does not exhibit any similarity with those of other elements in upper parts of the profile. However, in lower parts, the Th pattern is somehow like that of Zr (Fig. 8a) which may suggest its presence within the crystal lattice of zircon [21].
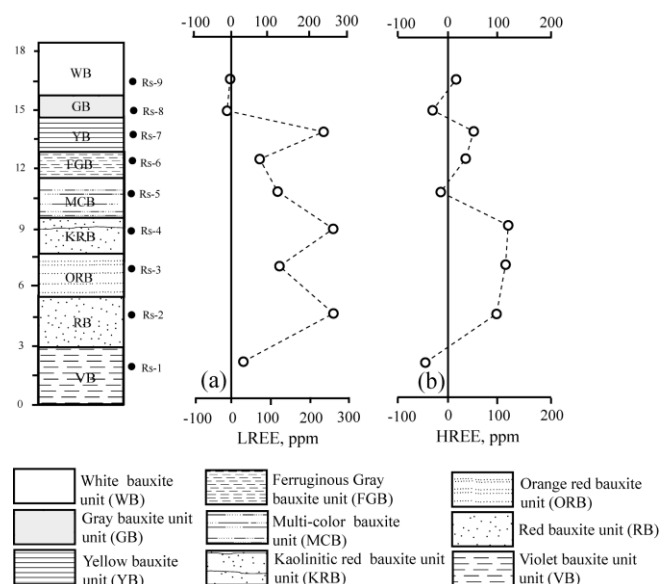
Figure 11. Mass change patterns for (a) LREE and (b) HREE arcoss the studied profile at Biglar.

Transition Trace Elements (V, Cr, Co, Ni)

V shows mass increase across the bauxite profile (Fig. 10a) while Cr, Co, and Ni depict both mass increase and decrease (Fig. 10b, c, d). Vanadium illustrates positive correlation with Al (R= 0.7) and negative with Si. Therefore, it can be inferred that the fixation of V in the weathered profile is related to the distribution of diaspore. The enrichment of Cr in the profile is probably controlled by iron oxide and hydroxides [14]. Studies done by Schwertmann and Pfab [26] revealed that Cr^{3+} could readily substitute for Fe^{3+} in the crystal lattice of hematite and goethite within the lateritic system. Ni correlates positively with SiO_2 (R= 0.75) and negatively with Fe_2O_3 (R= −0.35) which may be indicative of its fixation by the clay minerals. Co displays a good correlation with MnO (R= 0.69) and a poor one with Fe_2O_3 (R= 0.15). This may lead us to believe that Fe-bearing minerals did not play a significant role in controlling Co. In fact, Co distribution was substantially controlled by Mn-bearing minerals.

Rare Earth Elements (REEs)

The patterns of mass changes of LREEs (La-Gd) and HREEs (Tb-Lu) illustrate their overall increase in the upper parts of the studied profile (Fig. 11a, b). It seems that the presence of organic matters and their decay might have furnished conditions which led to leaching of REEs from the upper parts of the profile. Coupled downward percolation of acidic weathering solutions toward carbonate bedrock (as a buffering agent) and the fluctuations of water table brought about pH increase which was the principal factor for fixation of REEs within the profile [25, 27].

The Host Minerals for REEs

Many groups of minerals were suggested as potential hosts for REEs by many researchers. They include clay minerals (for both LREEs and HREEs) [7], secondary phosphate minerals (e.g., apatite) [2, 6], Mn-oxides and hydroxides [13], and Fe-oxides and hydroxides [23]. It should be noted that identification of minerals with abundance < 4% by XRD method is rather difficult. Therefore, in addition to the mineral phases identified by XRD in this study, other unidentified host minerals may also exist. In order to identify the potential host minerals for REEs, attempts have been made to accomplish Spearman,s rank correlation [24] among some constituent elements (Table 4). The correlation between REEs and Al is negative (R<−0.30) and between HREEs and Si is weakly positive (R= 0.1− 0.51). This attests to the fact that clay minerals in the residual units did not act as important concentrating agents for REEs. The weakly positive correlation between Fe and LREEs (R<0.35) implies that hematite, as a minor constituent mineral, played a role in concentrating LREEs. Nb and Zr show negative correlation with REEs (R < −0.25). This suggest that Nb- and Zr-bearing minerals (e.g., anatase and zircon)

Table 4. Spearman's rank correlation coefficients of major, minor, and trace elements with REEs in Biglar bauxite deposit

	SiO₂	Al₂O₃	Fe₂O₃	CaO	MgO	Na₂O	K₂O	TiO₂	P₂O₅	Ba	Zr	Y	Nb
La	0.10	-0.41	0.33	0.66	0.24	0.45	0.60	-0.76	0.66	0.85	-0.73	0.55	-0.31
Ce	-0.06	-0.30	0.35	0.55	0.29	0.5	0.60	-0.71	0.65	0.76	-0.66	0.5	-0.31
Pr	0.18	-0.66	0.31	0.58	0.17	0.24	0.63	-0.80	0.8	0.88	-0.71	0.81	-0.43
Nd	0.29	-0.59	0.30	0.68	0.18	0.51	0.60	-0.69	0.77	0.84	-0.62	0.79	-0.32
Sm	0.45	-0.68	0.1	0.51	0.04	0.09	0.50	-0.68	0.71	0.58	-0.55	0.78	-0.32
Eu	0.51	-0.53	-0.15	0.61	0.09	0.07	0.43	-0.58	0.73	0.5	-0.45	0.73	-0.46
Gd	0.45	-0.60	-0.11	0.58	0.07	0.22	0.57	-0.60	0.8	0.61	-0.43	0.83	-0.28
Tb	0.36	-0.63	-0.15	0.55	0.22	0.35	0.65	-0.63	0.88	0.61	-0.45	0.91	-0.28
Dy	0.28	-0.63	-0.10	0.50	0.22	0.37	0.65	-0.70	0.91	0.61	-0.53	0.96	-0.25
Ho	0.28	-0.66	-0.10	0.50	0.22	0.37	0.65	-0.70	0.91	0.61	-0.53	0.96	-0.31
Er	0.20	-0.66	-0.01	0.36	0.19	0.4	0.61	-0.78	0.90	0.53	-0.61	0.96	-0.31
Tm	0.20	-0.65	-0.01	0.36	0.19	0.34	0.61	-0.78	0.90	0.53	-0.61	0.96	-0.51
Yb	0.31	-0.69	-0.13	0.45	0.14	0.32	0.60	-0.71	0.88	0.55	-0.55	0.95	-0.40
Lu	0.34	-0.69	-0.19	0.49	0.16	0.36	0.64	-0.80	0.87	0.59	-0.64	0.92	-0.42

made no contribution for concentration of REEs. The correlation between Mn and REEs (R= 0.07−0.5) is weak which is indicative of the insignificant role of Mn oxides and hydroxides in concentrating of REEs. Phosphorus correlates positively well with REEs (R= 0.65−0.91) which suggests the significant role of P-bearing minerals in controlling partial distribution of REEs. Phosphorus also highly correlates with La, Ce, and Nd (R = >0.65). This provides us a reason to believe the presence of monazite and rhabdophane. Since Y shows well correlation with REEs (R= 0.5−0.96), it hints to the fact that the distribution of rare earth elements, in addition to the above phosphate minerals, was also controlled by xenotime.

Results

Biglar Permo-Triassic bauxite deposit consists of 8 discontinuous lenses developed along the contact of Ruteh (Permian) and Elika (Triassic) carbonate formations. Petrographical and mineralogical studies revealed that this deposit contains minerals such as diaspore, hematite, goethite, muscovite, feldspars, anatase, kaolinite, pyroxene, lepidochrosite, calcite, zeolite, and quartz which are derived from an authigenic origin. Incorporation of the obtained data from field and geochemical studies indicate that the organic matters and the carbonate bedrocks had profound effects on changing the chemistry of the weathering solutions and evolution of the weathered profile. Based upon the geochemical data, fixation in neomorph phases and

existing in the resistant mineral phases were the most important controlling factors for distribution of many trace and rare earth elements. In general, the obtained results demonstrate that the distribution and fixation of rare earth elements in the weathered profile was controlled chiefly by monazite, rhabdophane, belovite, and xenotime; Th by zircon; Y by xenotime and churchite; Zr, Hf, and Nb by zircon and anatase; U and Cr by hematite; Ga and V by diaspore; Rb and Ni by kaolinite; Sr by kaolinite and nordite; and Co by Mn-bearing oxides and hydroxides.

References

1. Balasubramaniam K.S., Surendra M., and Kumar T.V. Genesis of certain bauxite profiles from India. Chemical Geology, **60**: 227-235(1984).
2. Banifield J.F., and Eggleton R.A. Apatite replacement and REE mobilization, fractionation, and fixation during weathering, Clays and Clay Minerals, **37**: 113-127 (1989).
3. Bardossy G. Karst Bauxites. Elsevier Scientific, Amsterdam, 441p. (1982).
4. Bardossy G.Y., and Aleva, G.Y.Y. Lateritic Bauxites. Akademia, Kiado Budapest, 646 p. (1990).
5. Braun J.J., Ngoupayou J.R.N., Vires J., Dupre B., Bedimo J.P.B., Boeglin J.L., Robain H., Nyeck B., Freydier R., Nkamdjou L.S., Rouiller J., and Muller J.P. Present weathering rates in a humid tropical watershed: Nsimi, South Cameroon. Geochimica et Cosmochimica Acta, **69**: 357-387 (2005).
6. Braun J.J., Pagel M., Herbillon A., and Rosin C. Mobilization and redistribution of REEs and Th in a syenitic lateritic profile- a mass balance study.

Geochimica et Cosmochimica Acta, **57**: 4419-4434 (1993).

7. Condie K. Another look at REEs in shales. Geochimica et Cosmochimica Acta, **55**: 2527-2531 (1991).

8. Henderson P. Rare Earth Element Geochemistry. Elsevier, Amsterdam, 499 p. (1984).

9. Hill I. G. Worden R. H. G., and Meighan I. G. Geochemical evolution of a paleolaterite: the interbasaltic formation, Northern Ireland. Chemical Geology, **166**: 65-84 (2000).

10. Kangarani F., Calagari A. A., and Abedini A. Studies of mineralogy and elemental geochemistry of Biglar bauxite horizon (NW of Abgarm-Ghazvin province). Proceeding of the 11th Symposium of Geological Society of Iran, Ferdoosy University, 4-6 Sept, 2007, Mashhad, Iran (2007).

11. Kangarani F., Calagari A.A., and Abedini A. Minera-logical and geochemical controls on REE distribution during bauxitization processes at Biglar (NW of Abgarm-Gazvin province). Proceeding of the 15th Symposium of the Society of Crystallography and Mineralogy of Iran, Ferdoosy University, 13-14 Feb, 2008, Mashhad, Iran (2008).

12. Karadag M., Kupeli S., Arik F., Ayhan A., Zedef V., and Doyen A. Rare earth element (REE) geochemistry and genetic implications of the Mortas bauxite deposit (Seydisehir/Konya)-southern Turkey. Chemie der Erde-Geochemistry, **69**: 143-159 (2009).

13. Koppi A.J., Edis R., Foeld D.J., Geering H.R., Klessa D.A., and Cockayne D.J.H. REEs trends and Ce-U-Mn associations in weathered rock from Koongarra, northern territory, Australia. Geochimica et Cosmochimica Acta, **60**: 1695-1707 (1996).

14. Laskou M., and Economou-Eliopoulos M. The role of microorganisms on the mineralogical and geochemical characteristics of the Parnassos-Ghiona bauxite deposits, Greece. Journal of Geochemical Exploration, **93**: 67-77 (2007).

15. Lopez J. M. G., Bauluz B., Fernandez-Nieto C., and Oliete A. Y. Factors controlling the trace element distribution in fine-grained rocks: the Albian kaolinite-rich deposits of the Oliete Basin (NE Spain). Chemical Geology, **214**: 1-19 (2005).

16. Ma J., Wei G., Xu Y., Long W., and Sun W. Mobilization and re-distribution of major and trace elements during extreme weathering of basalt in Hainan Island, South China. Geochimica et Cosmochimica Acta, **71**: 3223-3237 (2007).

17. MacLean W. H., Bonavia F. F., and Sanna, G. Argillite debris converted to bauxite during karst weathering: evidence from immobile element geochemistry at the Olmedo deposit, Sardinia. Mineralium Deposita, **32**: 607-616 (1997).

18. Malpas J., Duzgoren-Aydin N.S., and Aydin A. Behaviour of chemical elements during weathering of pyroclastic rocks, Hong Kong. Environment International, **26**: 359-368 (2001).

19. Mameli P., Mongelli G., Oggiano G., and Dinelli E. Geological, geochemical and mineralogical features of some bauxite deposits from Nurra (western Sardinia, Italy): insights on conditions of formation and parental affinity. International Journal of Earth Sciences, **96**: 887-902 (2007).

20. Özlü N.Trace element contents of karst bauxites and their parent rocks in the Mediterranean belt. Mineralium Deposita, **18**: 469-476 (1983).

21. Panahi A.,Young G.M., and Rainbird R.H. Behavior of major and trace elements (including REE) during Paleoproterozoic pedogenesis and diagenetic alteration of an Archean granite near Ville Marie, Quebec, Canada. Geochimica et Cosmochimica Acta, **64** (13): 2199- 2220 (2000).

22. Plank T., and Langmuir, C.H. The chemical composition of subducting sediment and its consequences for the crust and mantle. Chemical Geology, **145**: 325-394 (1988).

23. Pokrovsky O.S., Schott J., and Dupre B. Trace element fractionation and transport in boreal rivers and soil porewaters of permafrost-domonated basaltic terrain in Central Siberia. Geochimica et Cosmochimica Acta, **70**: 3239-3260 (2006).

24. Rollinson H. Using geochemical data: evaluation, presentation, interpretation. Longman Scientific and Technical, 352 p. (1993).

25. Roy P.D., and Smykatz-Kloss W. REE geochemistry of the recent playa sediments from the Thar Desert, India: an implication to playa sediment provenance. Chime der Erde-Geochemistry, **67**: 55-68 (2007).

26. Schwertmann U., and Pfab G. Structural V and Cr in lateritic iron oxides: genetic implications. Geochimica et Cosmochimica Acta, **60**: 4279-4283 (1996).

27. Steinmann M., and Stille P. Rare earth element transport and fractionation in small streams of a mixed basaltic granitic catchment basin (Massif Central, France). Journal of Geochemical Exploration, **88**: 336-340 (2006).

28. Valeton I. Bauxites. Elsevier, 226 p. (1972).

29. White A. F., Bullen T. D., Schultz M. S., Blum A. E., Huntington T. G., and Peters N. E. Differential rates of feldspar weathering in granitic regoliths. Geochimica et Cosmochimica Acta, **65**: 847- 869 (2001).

30. Wimpenny J., Gannoun A., Burton K.W., Widdowson M., Jamed R.H., and Gilason S.R. Rhenium and osmium isotope and elemental behaviour of India. Earth and Planetary Science Letters, **261**: 239-258 (2007).

31. Winchester J.A., and Floyd P.A. Geochemical discrimination of different magma series and their differentiation products using immobile elements. Chemical Geology, **20**: 325-343 (1977).